JACS
JOURNAL OF THE AMERICAN CHEMICAL SOCIETY
pubs.acs.org/JACS
Article

Encapsulating Semiconductor Quantum Dots in Supramolecular Cages Enables Ultrafast Guest–Host Electron and Vibrational Energy Transfer

Shuai Lu,[‡‡] Darien J. Morrow,[‡‡] Zhikai Li, Chenxing Guo, Xiujun Yu, Heng Wang,* Jonathan D. Schultz, James P. O'Connor, Na Jin, Fang Fang, Wu Wang, Ran Cui, Ou Chen, Chenliang Su, Michael R. Wasielewski, Xuedan Ma,* and Xiaopeng Li*

Cite This: *J. Am. Chem. Soc.* 2023, 145, 5191–5202

ABSTRACT: In the field of supramolecular chemistry, host–guest systems have been extensively explored to encapsulate a wide range of substrates, owing to emerging functionalities in nanoconfined space that cannot be achieved in dilute solutions. However, host–guest chemistry is still limited to encapsulation of small guests. Herein, we construct a water-soluble metallo-supramolecular hexagonal prism with a large hydrophobic cavity by anchoring multiple polyethylene glycol chains onto the building blocks. Then, assembled prisms are able to encapsulate quantum dots (QDs) with diameters of less than 5.0 nm. Furthermore, we find that the supramolecular cage around each QD strongly modifies the photophysics of the QD by universally increasing the rates of QD relaxation processes via ultrafast electron and vibrational energy transfer. Taken together, these efforts expand the scope of substrates in host–guest systems and provide a new approach to tune the optical properties of QDs.

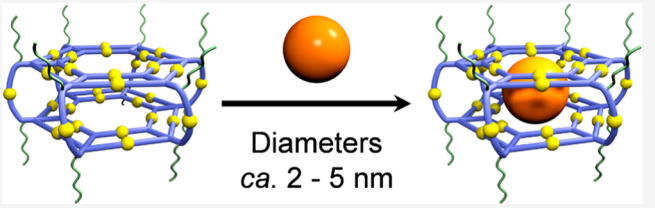

INTRODUCTION

Since the discovery of crown ethers half a century ago,[1] substantial efforts have been made with the goal of developing artificial molecular nanospaces, such as cyclodextrins,[2] calixarenes,[3] cucurbiturils,[4] and pillararenes,[5] to explore host–guest chemistry. In addition to covalent macrocycles, a variety of polycyclic architectures or three-dimensional (3D) covalent containers also emerged after the pioneering discovery of cryptands[6] and spherands[7] via either multistep synthesis[8] or one-step dynamic covalent chemistry.[9] Despite the rapid growth of covalent macrocycles and containers, the encapsulation substrates available for host–guest chemistry have been limited to small molecules and ions.[10−12] In order to encapsulate larger guest molecules, multiple, cooperative hydrogen bonding interactions have been employed to engineer supramolecular capsules and cages with increasing size.[13] More recently, coordination-driven self-assembly of metallo-supramolecular cages has continuously pushed the limits of non-covalent containers in terms of size, complexity, and diversity.[14] To date, the largest reported metallo-supramolecular cages have a sub-10 nm diameter.[14i]

Even with the wide array of available molecular and supramolecular hosts, fullerenes have remained the largest guest substrates for the past 3 decades[15−17] because the assembled hosts do not have sufficient binding forces to trap larger substrates. In a few cases, such as the encapsulation of small proteins within metallo-supramolecular cages, covalent bonds are required to anchor the protein to the host backbone.[18] A similar covalent/coordination anchoring strategy has been applied for the growth of nanoparticles within host cavities.[19] Looking beyond small molecules as guests, encapsulation of other substances, for instance nanoparticles, remains a formidable challenge which cannot be overcome by a simple extension of conventional host–guest chemistry. The encapsulation of nanoparticles in supramolecular cavities is poised for expanding the host–guest functionalities beyond proceeding analogues. Among the various types of nanoparticles, semiconductor quantum dots (QDs)[20] and metal nanoparticles[21] have attracted substantial attention due to their distinctive, tunable optical properties. Moreover, the optical properties of QDs within a confined space can be reshaped by their intimate interactions with the hosts. Acceptor–donor systems built around QDs and metal nanoparticles display size- and shape-dependent charge and energy transfer processes,[22] which can be further regulated by the local environment surrounding the nanoparticles.[23] Particularly, encapsulation of a nanoparticle within a host should allow precise control over

Received: November 13, 2022
Published: February 6, 2023

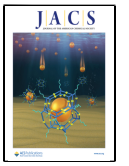

https://doi.org/10.1021/jacs.2c11981
J. Am. Chem. Soc. 2023, 145, 5191–5202

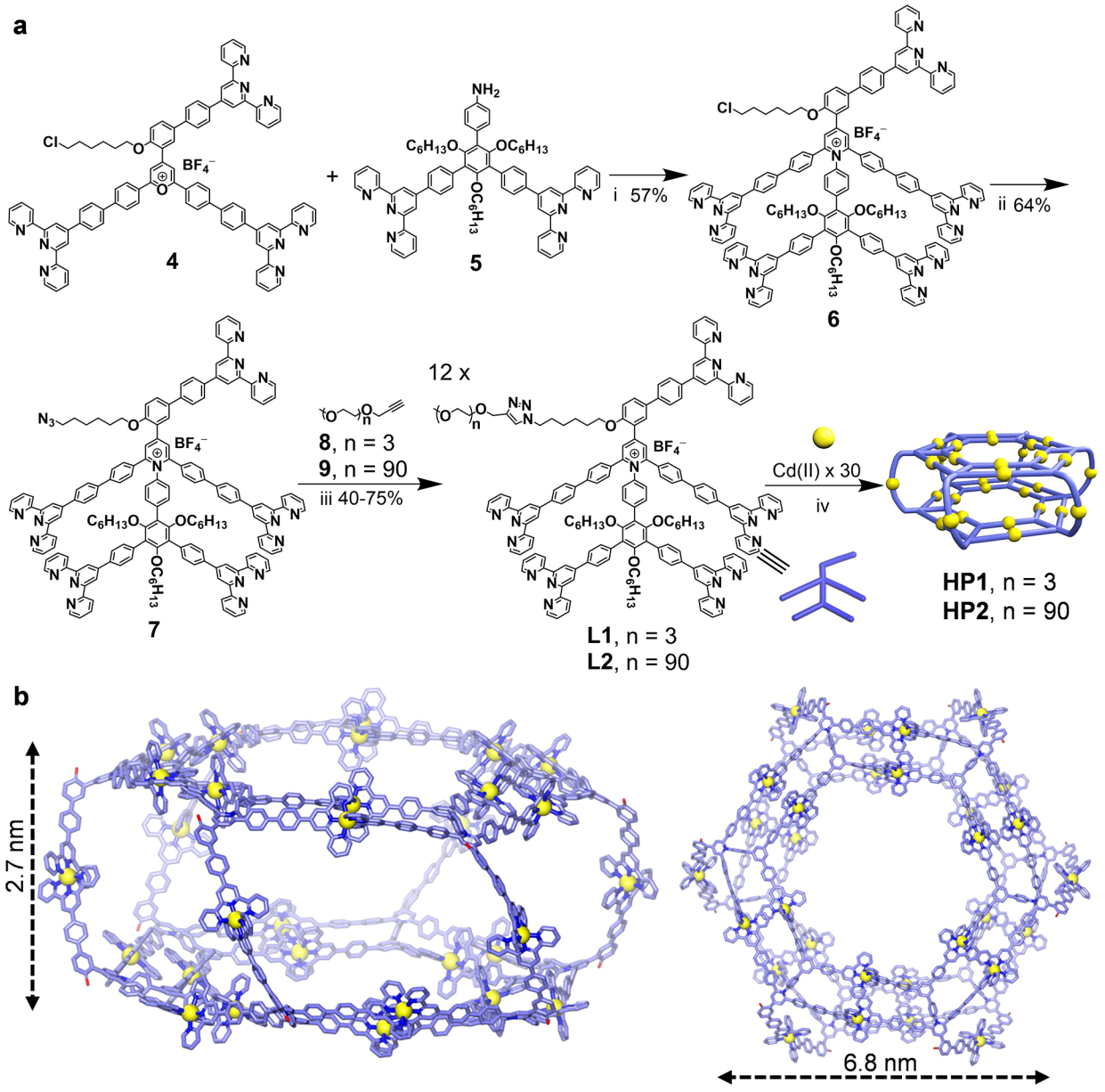

Figure 1. (a) Synthesis of ligands **L1** and **L2** and coordination-driven self-assembly of hexagonal prisms **HP1** and **HP2**. (b) Molecular modeling of **HP1** (ethylene glycol and alkyl chains are omitted for clarity). Conditions: (i), 4 Å molecular sieves, dimethyl sulfoxide (DMSO), 90 °C, 24 h. (ii), NaN_3, *N*,*N*-dimethylformamide (DMF), 90 °C, 36 h. (iii), CuBr, *N*,*N*,*N*′,*N*′,*N*″-pentamethyl diethylene triamine (PMDETA), DMF, 50 °C, 24 h. (iv) DMSO, 80 °C, 12 h.

transfer processes between them. However, it remains a longstanding challenge to construct discrete nanospaces with molecular precision to encapsulate nanoparticles and explore the photophysics of host−guest complexes.

Here, we report an alternative yet widely applicable strategy for encapsulating inorganic nanoparticles in supramolecular cavities by leveraging the hydrophobic effect. A giant water-soluble supramolecular host system with a large hydrophobic interior is constructed by introducing multiple polyethylene glycol (PEG) chains into the framework of terpyridine (TPY)-based metallo-supramolecular hexagonal prisms. Such a design of the host allows the selective encapsulation and confinement of hydrophobic QDs with diameters less than 5.0 nm in the supramolecular cavity. To unveil the interactions between the supramolecular hosts and QD guests, we employ a suite of optical measurements spanning femtosecond to microsecond time scales. We discover that the intimate contact between the supramolecular hexagon cavities and QDs transforms the photophysical properties of the latter through ultrafast electron transfer. Moreover, the supramolecular cages can serve as passivation layers and accelerate hot carrier cooling in the QDs, likely through near-field vibration mode coupling to the lattice phonons of the QDs. These findings reveal that a marriage between supramolecular systems and inorganic nanoparticles expands the canon of the complex functionality by encompassing the organic and inorganic chemistries, as well as opening the door for a paradigmatic shift in the design of host−guest systems for various types of applications.[24]

RESULTS AND DISCUSSION

Synthesis and Characterization of Supramolecular Hexagonal Prisms. In a previous study, we constructed a

https://doi.org/10.1021/jacs.2c11981
J. Am. Chem. Soc. 2023, 145, 5191−5202

hexagonal prism by assembling 12 pentatopic TPY ligands with 30 metal ions.[25] In this work, we design supramolecular prisms with hydrophobic interiors and hydrophilic exteriors by introducing different lengths of ethylene glycol chains onto the pentatopic TPY ligands **L1** and **L2** via a "click" reaction (Figure 1a and Schemes S1 and S2 for details). Such multiarmed building blocks with multiple tridentate TPY moieties afford enhanced coordination stability, which ensures the structural integrity of assemblies with long PEG chains. **L1** linked with an oligomer of ethylene glycol is synthesized as a model system for self-assembly of supramolecular prism to facilitate full characterization by nuclear magnetic resonance (NMR) spectroscopy and mass spectrometry (MS) (Figures S14–S25 and S28–S29), while **L2** with long PEG chains is used to further improve the water solubility of prism for the encapsulation of QDs.

HP1 and **HP2** are constructed by self-assembly of Cd(II) with **L1** and **L2**, respectively, in DMSO at 80 °C for 12 h with a ratio of 5:2 (Figure 1a). After that, electrospray ionization MS (ESI-MS) of **HP1** shows a dominant set of peaks with continuous charge states ranging from 17 + to 23 + due to the successive loss of the counterion (Figure 2a). The average

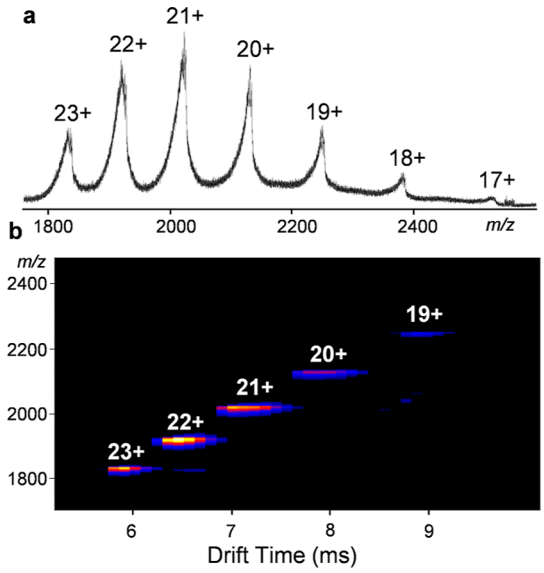

Figure 2. (a) ESI-MS and (b) TWIM-MS plots (*m/z* vs drift time) of **HP1**.

molar mass of **HP1** is deduced to be 45502 Da, matching well with the molecular formula of $[C_{2088}H_{1872}Cd_{30}F_{432}N_{228}O_{96}P_{72}]$. Traveling wave ion mobility MS (TWIM-MS) of **HP1** shows a series of bands with a narrow drift time at each charge state,[26] indicating that no other isomers or structural conformers exist (Figure 2b). However, ESI-MS only exhibits unresolved signals with severe superimposition for **HP2** because of the polydisperse nature of the 12 long PEG chains and multiple charges on the backbone (Figure S43).

Further evidences for the formation of the desired supramolecular structure are provided by detailed NMR studies (Figure 3a). When compared with the proton signals of **L1**, the ^{1}H NMR spectrum of **HP1** shows a broad pattern, suggesting the formation of large complexes. After self-assembly, the signals of TPY-$H^{a,b,c3',5'}$ protons display characteristic downfield shifts. Assignments of the other signals

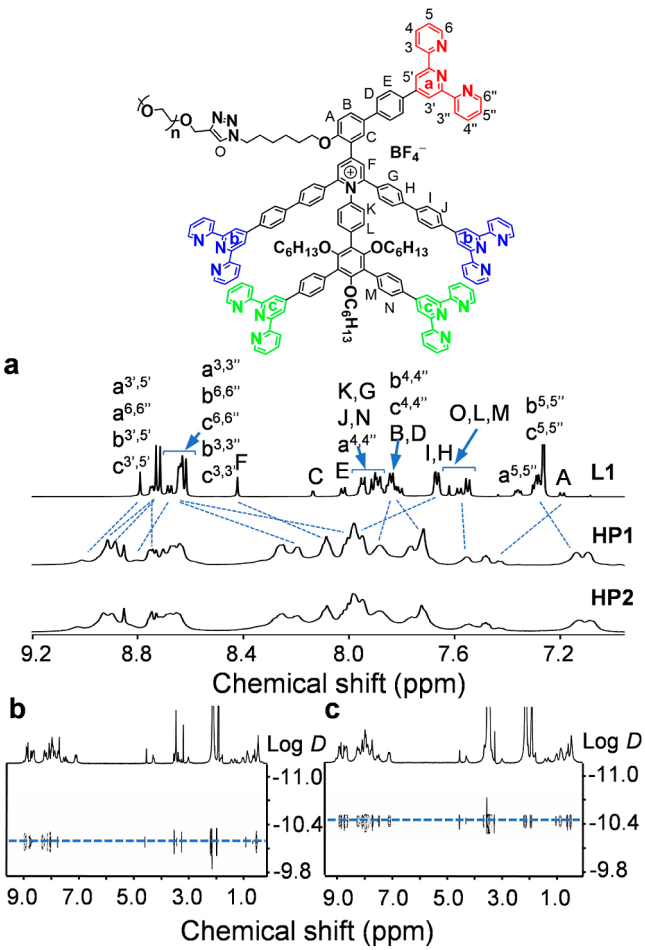

Figure 3. (a) ^{1}H NMR spectra (600 MHz, 300 K) of **L1** in $CDCl_3$, **HP1** in CD_3CN, and **HP2** in CD_3CN. DOSY spectra of (b) **HP1** and (c) **HP2** in CD_3CN.

are assisted by 2D correlation spectroscopy (2D COSY) and 2D nuclear Overhauser enhancement spectroscopy (2D NOESY) NMR (Figures S31–S34). Moreover, 2D diffusion-ordered spectroscopy (2D DOSY) of **HP1** exhibits a single band at log D = −10.18, indicating the formation of a discrete structure (Figure 3b). **HP2** shows similar sets of ^{1}H NMR spectrum as **HP1** (Figure S35) and 2D DOSY signal at log D = −10.44, corresponding to a larger assembled structure (Figure 3c) because of the long PEG chains. The assembled supramolecular prism has a hydrophobic cavity with an external diameter of around 6.8 nm according to molecular modeling (Figure 1b, disordered PEG chains were not taken into account during the simulation). The introduction of 12 long PEG chains to the framework of supramolecule **HP2** renders its exterior hydrophilicity and well solubility in CH_3CN/H_2O (v/v, 1:4) mixtures.

Size-Selective Separation of QDs. In this work, we utilize CdSe/CdS core/shell QDs as proof-of-concept inorganic guests on account of their high relevance to biolabeling and photocatalysis.[27] Considering that the diameters of the base face windows and the internal cavity of the metallo-supramolecular prism are estimated as ca. 3.0 and 5.0 nm (Figure S57), respectively, we reasoned that only QDs with a suitable size could fit in the inner space of the cavity (Figure 4a). To explore the size selectivity of encapsulation, QDs with broad size distributions ranging from 2–9 nm were

https://doi.org/10.1021/jacs.2c11981
J. Am. Chem. Soc. 2023, 145, 5191−5202

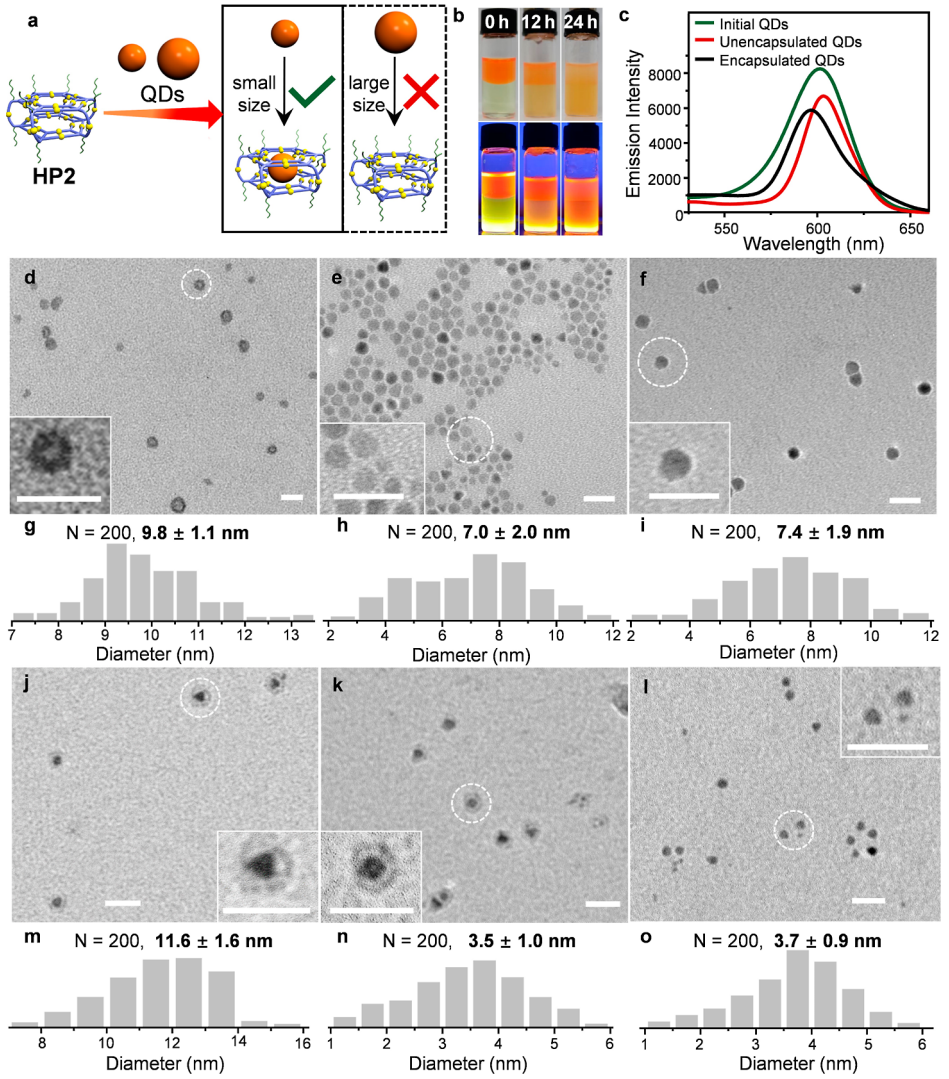

Figure 4. Size-selective encapsulation of QDs by HP2. (a) Cartoon representation of the size-selective encapsulation of QDs in **HP2**. (b) Photographs of the encapsulation process via extracting QDs from the *n*-hexane phase to a CH_3CN/H_2O (v/v, 1:4) solution of **HP2** at 0, 12, and 24 h, at room temperature; the top photograph was taken under ambient light, and the bottom photograph was taken in the dark upon illumination by a UV lamp with an excitation wavelength of 365 nm. (c) Fluorescence spectra of the initial QDs (0.02 mg/mL, green line), the remaining QDs in the upper layer after extraction (ca. 0.01 mg/mL, red line), and the isolated QDs (ca. 0.01 mg/mL, black line) after disassembling **HP2**. All QD samples were dissolved in *n*-hexane, and the excitation wavelength was 510 nm. TEM images of (d) **HP2**; (e) initial QDs; (f) QDs in the upper layer after extraction; (j,k) **HP2**⊃QDs in the bottom layer after extraction; and (l) QDs isolated from **HP2**⊃QDs complexes after the disassembly of **HP2** (insets display the enlarged images; scale bar, 20 nm). Diameter histogram of 200 individual dots shown in the TEM images (Figures g–i, m–o, and S45–S50): (g) **HP2**; (h) initial QDs; (i) QDs in the upper layer after extraction; (m) **HP2**⊃QDs; (n) QDs encapsulated inside **HP2**; and (o) separated QDs after disassembling **HP2**.

prepared for the following studies (Figures 4e and S47).[28] With oleic acid passivation layers on the surface, the QDs are insoluble in polar solvents like CH_3CN or water. Upon mixing **HP2** in CH_3CN/H_2O (v/v, 1:4) with QDs dispersed in *n*-hexane, a gradual transfer of the QDs from the upper layer to the bottom layer could be clearly observed by tracing the characteristic absorption and emission of QDs (Figure 4b), suggesting the possible encapsulation of QDs in **HP2** (see more details in the Supporting Information).

Fluorescence (FL) spectra were then collected to characterize the QDs before and after the encapsulation. The FL spectrum of the initial QDs solution showed a broad band centered at ca. 601 nm, with a full width at half-maximum (FWHM) as ca. 39 nm (Figure 4c). After extraction, the unencapsulated QDs that remained in the upper layer exhibited a narrower curve peaked at ca. 604 nm, with an FWHM estimated as 29 nm, indicating that the unencapsulated QDs have a larger size and narrower distribution than the initial nanoparticles. By treating the bottom layer with sodium bicarbonate to dissociate **HP2**, the encapsulated QDs were isolated and characterized by FL spectroscopy as well. Compared with the spectra of the initial and unencapsulated QDs, the emission curve of isolated QDs displays a blue-shift around 5 nm, and the FWHM value is estimated as 34 nm, indicating the smaller size of the corresponding QDs. Control experiments were also performed by using **L2** solution or pure CH_3CN/H_2O as the extraction phase, respectively. Both the control groups did not extract any QDs from the upper layer, without showing any color change in the extraction phase revealed by the photographs (Figure S44a,b). More control

https://doi.org/10.1021/jacs.2c11981
J. Am. Chem. Soc. 2023, 145, 5191−5202

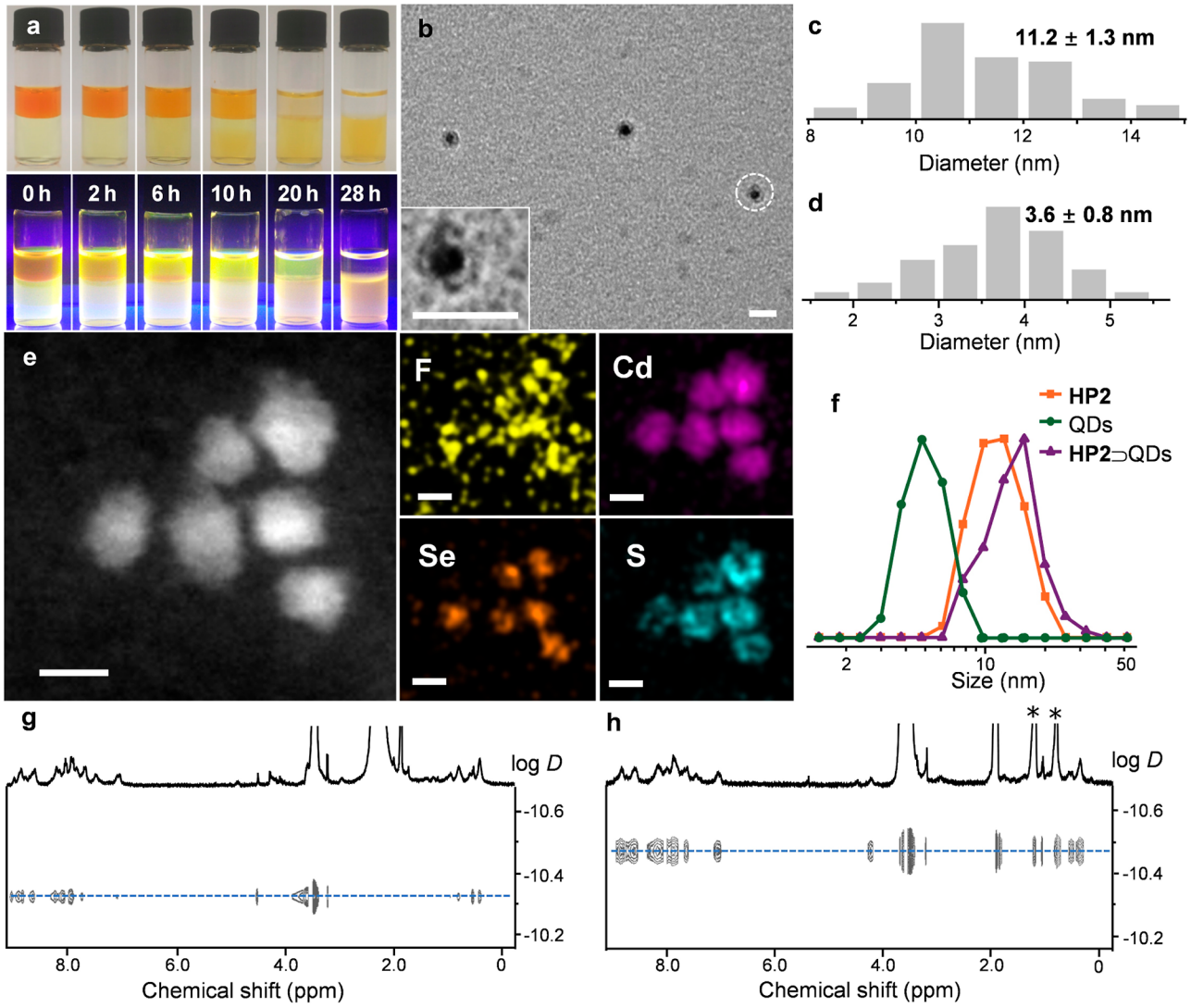

Figure 5. Characterizations of QDs (ca. 3.7 nm) and HP2⊃QDs complexes. (a) Photographs of the encapsulation process via extracting 3.7 nm QDs from the *n*-hexane phase to a CH_3CN/H_2O (v/v, 1:4) solution of **HP2** from 0 to 28 h at room temperature; the top photograph was taken under ambient light, and the bottom photograph was taken in the dark upon illumination by a UV lamp with an excitation wavelength at 365 nm. (b) TEM image of **HP2**⊃QDs (enlarged images are displayed in insets, scale bar, 20 nm). Diameter histogram of 200 individual dots shown in the TEM images correspondingly (c,d, and S52): (c) **HP2**⊃QDs; and (d) QDs encapsulated inside **HP2**. (e) High-angle annular dark-field scanning transmission electron microscopy (HAADF-STEM) image and the corresponding energy-dispersive X-ray spectroscopy (EDS) mapping images of a randomly selected region containing the **HP2**⊃QDs complexes, scale bar, 5 nm. (f) Dynamic light scattering (DLS) results of **HP2**, QDs, and **HP2**⊃QDs. DOSY spectra of (g) **HP2** in CD_3CN/D_2O (v/v, 1:4) and (h) **HP2**⊃QDs in CD_3CN/D_2O (v/v, 1:4); * labeled peaks are ascribed to oleic acid.

experiments were carried out by mixing **L2** and QDs in their common good solvents ($CHCl_3$/toluene, v/v, 4:1). After mixing **L2** and QDs, the characteristic absorption bands and emission peaks of QDs did not change significantly (Figure S59a,b), and no proton resonance peak shift of **L2** was observed in the ^1H NMR spectrum (Figure S41), indicating that no ligand exchange could occur between **L2** and QDs. All these results suggest that **HP2** can selectively encapsulate QDs according to their sizes, that is, the large QDs are unable to be hosted by **HP2** and mainly stay in the upper layer, while the small ones can be encapsulated and dispersed in the aqueous phase.

Transmission electron microscopy (TEM) was then applied to further prove the formation of **HP2**⊃QDs, and the size selectivity of the host−guest chemistry. First, doughnut-like structures of empty **HP2** are clearly observed in TEM images (Figures 4d and S46a−e), with average inner and outer diameters around 4.5 ± 0.7 nm and 9.8 ± 1.1 nm, respectively (Figures 4g and S46f). The measured inner diameter agrees well with the theoretically estimated cavity size (Figures 1b and S57), while the outer diameter is larger than the simulated value, owing to the PEG chains were not taken into account during the simulation. After extraction, the QDs in the upper layer have an average diameter of ca. 7.4 ± 1.9 nm, revealed by TEM observations (Figures 4f,i, and S49). The value is slightly larger than that of the initial QDs (7.0 ± 2 nm, Figures 4e,h, and S47), agreeing well with the FL results. Additionally, encapsulation of the QDs in **HP2** is clearly visible in the TEM images of the samples collected from the bottom layer (Figures 4j,k, and S48). The high-contrast QDs are mainly located in the center of doughnut-like **HP2** structures with relatively low contrast. Although some of the hosts are observed to be

https://doi.org/10.1021/jacs.2c11981
J. Am. Chem. Soc. 2023, 145, 5191−5202

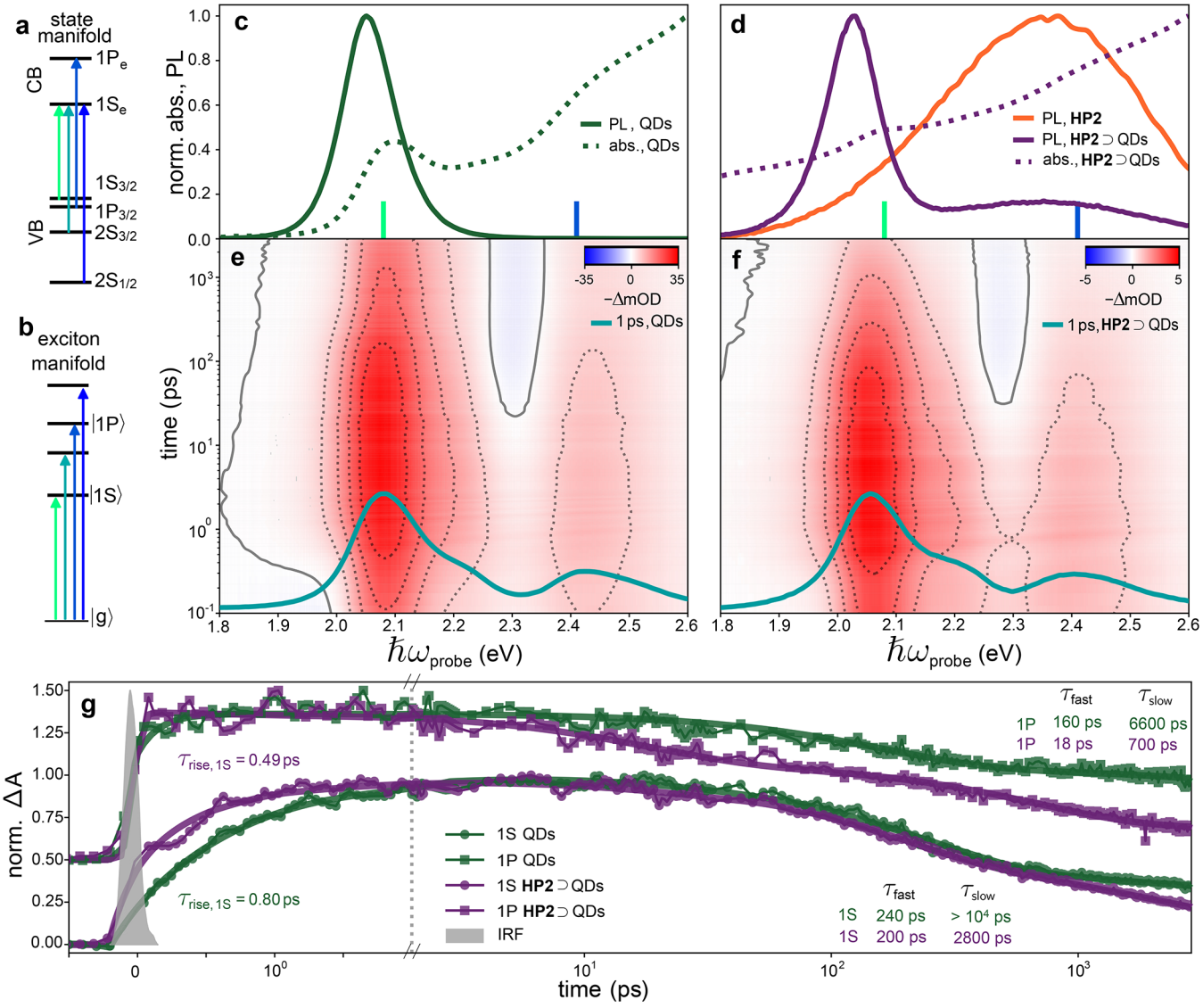

Figure 6. Steady state and ultrafast optical characterization (a) Energy levels of QDs (ca. 3.7 nm). in the state and (b) the exciton basis. (c) Absorption and photoluminescence spectra of bare QDs. (d) Absorption and photoluminescence spectra of **HP2**⊃QDs, as well as the PL spectrum of **HP2**. TA spectra of bare QDs (e) and **HP2**⊃QDs (f) after excitation by 2.92 eV pulses. The temporal axis is logarithmic. The curves are linecuts at a time delay of 1 ps. The average number of carriers per QD is kept below 0.5 to minimize many−body interactions. The most prominent 1S and 1P transitions are correspondingly marked in (c) and (d). (g) Temporal slices of the 1S and 1P bleach features from (c) and (d). Solid lines are fits based on an exponential growth and biexponential decay model convolved with the instrument response function (IRF, gray). Note that the *x*-axis is linear for time <2 ps and logarithmic for time >2 ps.

aggregated together, each of them contains QDs. The aggregation might take place in the solution or during the sample preparation stage when the solvent is removed, perhaps driven by the interactions among PEG chains of different cages.

Further examination of the TEM images reveals that in most **HP2**⊃QDs complexes, only one QD with a comparable size to the cavity is observed (Figures 4j,k, and S48). However, out of our expectation, some supramolecular prisms are found to host two or three QDs with a size of ca. 2 nm (Figure 4k). We speculate that two or three small QDs could be aggregated together within one host. As a result, **HP2** can selectively encapsulate QDs with a diameter below 5.0 nm. It is worth noting that some of the encapsulated QDs have a larger size than the diameter of the base face windows. These QDs could enter the cavity through the mechanism of partial dissociation of the metallo-cage (Figure S58),[29] owing to the dynamic nature of coordination bonds. After the dissociation of **HP2**, the QDs can be isolated, and their sizes are measured as ca. 3.7 ± 0.9 nm by TEM (Figures 4j−o, S48 and S50). Therefore, our metallo-supramolecular system provides a potential platform for separating QDs according to their sizes.

Photophysics of HP2⊃QDs Complexes. According to the previous observations, we can draw the conclusions that (i) the QDs with sizes above the cut-off diameter cannot be encapsulated; and (ii) the QDs with too small sizes result in the co-encapsulation of multiple particles. To simplify the system for further photophysical studies, we synthesized QDs with an average diameter of 3.7 nm as the guest.[28] A similar encapsulation process was performed in a biphasic system. The gradual transfer of the QDs from the upper *n*-hexane phase to the bottom CH_3CN/H_2O layer can also be clearly observed

https://doi.org/10.1021/jacs.2c11981
J. Am. Chem. Soc. 2023, 145, 5191−5202

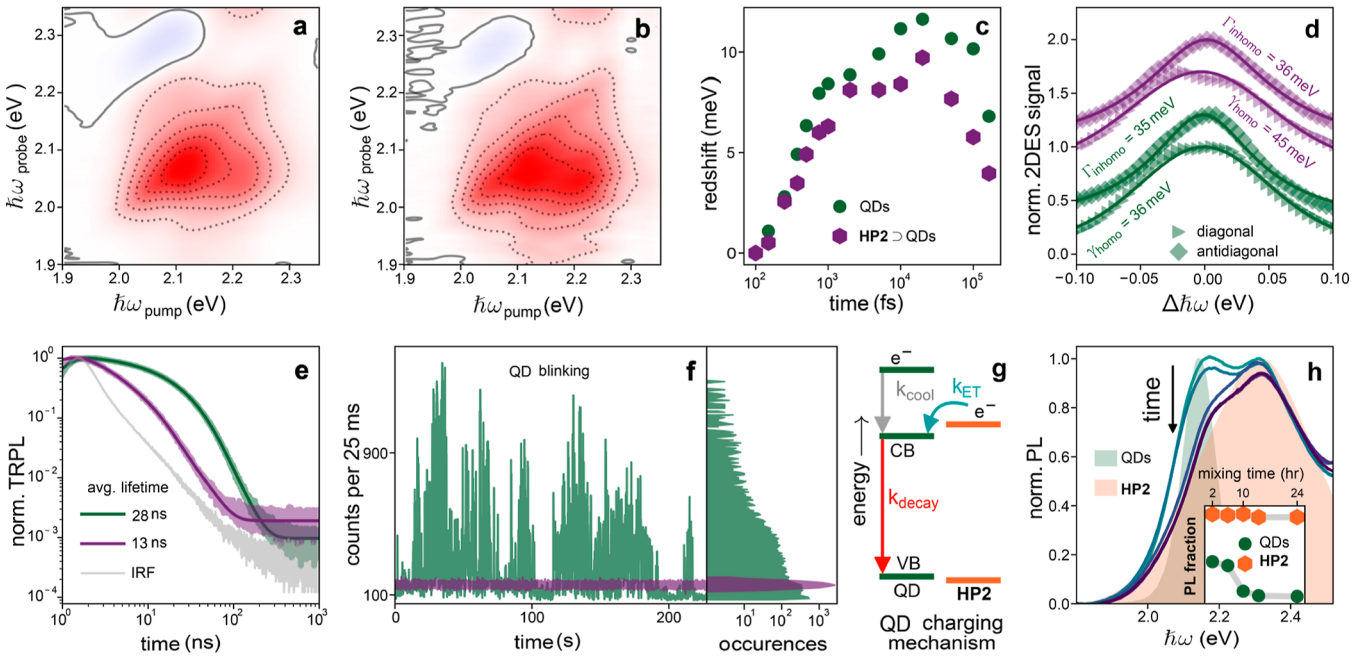

Figure 7. Two-dimensional electronic spectroscopy (2DES) and time-resolved photoluminescence (TRPL) measurements. 2DES responses of bare QDs (ca. 3.7 nm) (a) and **HP2**⊃QDs (b) 100 fs after excitation by a broadband pump. (c) Red-shift of the bleach maximum at different waiting times for a pump energy of 2.27 eV. Because the QD data always shows a larger red shift, there is no FRET from **HP2** to the QDs. (d) Normalized diagonal and antidiagonal cuts of 2DES responses that are corrected for non-uniform pump intensity at a pump−probe waiting time of 500 fs. Solid lines are fits using the model described in ref 42. QDs (**HP2**⊃QDs) have a homogenous linewidth of 36 meV (45 meV) and an inhomogeneous linewidth of 35 meV (36 meV). (e) TRPL curves excited with 2.82 eV pulsed light and collected with a 2.07 eV bandpass filter on a double-logarithmic scale. IRF is shown in gray. Solid lines are fits using a triexponential decay model convolved with the IRF. (f) Left: time-dependent PL intensities of a bare QD (green) and a QD in **HP2** (purple). Right: the corresponding count rate histograms. The weakly emissive and non-blinking "gray" states observed for the **HP2**⊃QDs provide further evidence of QD charging. (g) Sketch of QD charging and decay mechanism. (h) PL spectra of **HP2** (orange) and QD (green) mixture as a function of mixing time. The inset shows how the QD PL is quenched with the mixing time.

(Figure 5a). It is worth noting that the characteristic color of the QDs in the upper layer was completely faded after 28 h, suggesting that all the QDs were encapsulated. In sharp contrast, when 5.7 nm QDs were used, negligible color change was observed in the CH_3CN/H_2O phase (Figure S44c), indicating the size was beyond the accessible range for the encapsulation, further confirming the size selectivity of this host−guest system.

To confirm the encapsulation, we performed detailed TEM, STEM, DLS, atomic force microscopy (AFM), and NMR studies of the bottom layer containing the putative host−guest complexes of **HP2** and 3.7 nm QDs. **HP2** dissolved in CH_3CN/H_2O (v/v, 1:4) and 3.7 nm QDs dissolved in *n*-hexane are used as the references. Encapsulation of 3.7 nm QDs (Figure S51) in **HP2** could also be clearly observed in the TEM images (Figures 5b and S52). Due to the comparable sizes of the supramolecular cavity and QDs, each **HP2** contains one QD on average. After encapsulation, the average size of the complexes is expanded from 9.8 ± 1.1 nm to 11.2 ± 1.3 nm (Figures 4g and 5c). The QDs inside the complexes have the diameters of 3.6 ± 0.8 nm (Figure 5d). EDS mapping shows the distributions of characteristic elements as expected (Figures 5e and S53). For instance, Se is only observed in the inner core of the observed dots; S is dispersed in the shell out of the CdSe core; F from the counterion of **HP2** (i.e., PF_6^-) is mainly observed in the outer rim surrounding the QDs; Cd, an element that is contained by both QDs and **HP2**, is found across the whole area of the dots (Figures 5e and S53). DLS also confirms the formation of **HP2**⊃QDs by showing an expansion in size from 13.4 ± 1.1 nm to 15.7 ± 2.1 nm (Figure 5f). Moreover, AFM reveals a series of dots with 3.3 ± 0.6 nm in height and concave centers for **HP2** (Figure S54). In contrast, AFM measurements of **HP2**⊃QDs show they are not concave-shaped and have an increased height of 5.0 ± 1.0 nm, further indicating the encapsulation of QDs within cages (Figure S56).

^{1}H NMR spectra of **HP2** in CD_3CN/D_2O (v/v, 1:4) under various concentrations did not display any fragment signals, suggesting the stability of **HP2** under the encapsulation condition (Figure S40). Moreover, the spectra of **HP2** before and after the encapsulation did not show obvious changes in the aromatic region (Figure S42), confirming the integrity of the supramolecular backbone during the host−guest process without obvious decomposition. Finally, 2D DOSY was performed for both **HP2** and **HP2**⊃QDs in CD_3CN/D_2O (v/v, 1:4). After encapsulation, oleic acid displays signals at the same band with the **HP2** signals, indicating the successful encapsulation of QDs in **HP2** (Figure 5g,h). It also reveals that oleic acids that undergo phase transfer still stay on the QDs' surface after the encapsulation. We propose that these surface ligands with long aliphatic chains play a key role in the host−guest process and could provide van der Waals attractions with the hexyloxy moieties on **HP2** to facilitate the encapsulation and stabilize the formed complexes.[30] After encapsulation, 2D DOSY spectrum of **HP2**⊃QDs shows a single band at log D = −10.48, smaller than log D = −10.33 of **HP2**. These results are in accordance with the expected increase in size of **HP2**⊃QDs after complexation. As a result, through monitoring the 2D

https://doi.org/10.1021/jacs.2c11981
J. Am. Chem. Soc. 2023, 145, 5191−5202

DOSY spectra of the complexation solution, a **HP2**⊃QDs sample with a negligible amount of free **HP2** can be obtained.

The successful encapsulation of QDs (ca. 3.7 nm) into **HP2** provides us an ideal platform for interrogating the energetics and carrier dynamics of QDs in a precisely confined nanospace, which may feature host−guest electron and energy communication. Due to quantum confinement, the band structures of QDs are composed of discrete energy levels (Figure 6a). Optical transitions among these energy levels give rise to excitonic states, with the most prominent being the 1S ($1S_{3/2} \rightarrow 1S_e$) and 1P ($1P_{3/2} \rightarrow 1P_e$) transitions (Figure 6b). Upon encapsulation of 3.7 nm QDs with **HP2**, the originally distinct absorption peak of the former (Figure 6c) becomes obscured (Figure 6d). The emission spectrum of **HP2**⊃QDs comprises two major peaks (Figure 6d): a sharp peak at 2.05 eV from the QDs and a broad peak at 2.4 eV associated with metal-to-ligand charge-transfer (MLCT) states in **HP2**.[31]

To unveil the effects of encapsulation on the QDs' carrier dynamics, we use ultrafast transient absorption (TA) spectroscopy to investigate the generation and subsequent decay of electrons in conduction bands.[32] Figure 6e,f show the TA spectra of QDs and **HP2**⊃QDs, respectively, as a function of time following excitation with ultrafast 2.92 eV pulses. The rate that hot electrons cool and occupy the 1S state is faster for encapsulated QDs than for bare QDs (0.49 ps vs 0.80 ps, Figure 6g). Moreover, the biexponential relaxation dynamics of both 1S and 1P electron states are significantly faster for encapsulated QDs. A similar increase in relaxation rate upon encapsulation is observed in time-resolved photoluminescence (TRPL) experiments (Figure 7e) where the triexponential, weighted-average luminescent lifetime changes from 28 to 13 ns following the encapsulation of QDs into **HP2**.

There are primarily three possible mechanisms which could be responsible for the increase of carrier filling rate upon encapsulation of QDs: (i) a change in QDs' passivation and surface-trap density due to **HP2** overlayer, (ii) Förster resonance energy transfer (FRET) between the excited MLCT states of **HP2** and QDs, and (iii) charge injection from **HP2** to QDs.

Hot electrons in QDs relax to the band edge by an Auger-like mechanism where electrons transfer excess energies to holes, followed by the subsequent fast hole relaxation through their dense spectrum of states. It is known that changes to the QDs' surface do not affect hole trapping/relaxation rates.[32] As such, passivation and trapping cannot explain the increase in the 1S filling rate upon encapsulation.

Although the **HP2**⊃QDs system fulfills the two criteria for FRET to occur, that is, an overlap between **HP2** emission and QDs absorption, and their close enough distance,[33] our two-dimensional electronic spectroscopy (2DES) measurements exclude FRET. Specifically, if FRET exists, it would be manifested in the 2DES map along the probe axis as a smoothly red shifting peak from the acceptor absorption maximum at early times to the donor emission maximum at late times.[33] Figure 7a,b shows slices from our 2DES datasets at a pump−probe waiting time of 100 fs (see Figures S61−S63 for full datasets). The diagonal bleach features along with crosspeaks indicate rapid bleaching of band edge states from resonant and hot excitation, respectively. Figure 7c shows how the bleach feature along the probe axis red-shifts due to thermalization and cooling. Notably, QDs in **HP2** exhibit less red-shifting than non-encapsulated QDs. This suggests that FRET is not present within the pump energy range employed in our measurements. This lack of FRET might be due to the weak emission of the short-lived MLCT states,[31b,c,34] as well as the random orientations of the optical transition dipoles in the encapsulated QDs,[35] with respect to the MLCT states.

The existence of charge transfer between **HP2** and QDs (Figure 7g) is confirmed by monitoring the time-dependent PL spectra of the **HP2**⊃QDs species during their encapsulation process (Figure 7h). **HP2** emission decreases slightly in intensity while QDs emission is heavily quenched, evident of charge transfer-induced quenching. Moreover, our single QDs measurements show that bright, band edge emission from the QDs with characteristic on−off blinking (Figure 7f, green) is changed upon encapsulation to a weakly emissive, rapidly decaying gray state with suppressed blinking (Figure 7f, purple, see Figure S67 for second-order photon correlation spectroscopy). Suppressed blinking and increased relaxation rates are indicative of charged exciton formation in QDs, which in this case is mediated by **HP2**.[36] Given the relative energy levels of the QD band edges,[37] and the excited state redox potentials of the TPY-Cd(II) complexes derived from the emission maximum and ground state redox couple (Figure 7g),[38] we attribute this charging channel to electron injection from the TPY-Cd(II) complexes to the QDs, probably through a hopping mode.[39] By fitting the 2DES datasets (see fitting details in Supporting Information), the average charge transfer rate from **HP2** to QDs is estimated to be $k_{CT} = 1/330\ fs^{-1}$ (see Figure S66). Note that the rate decreases as the pump frequency increases; this correlates with our TA observations which use a larger excitation frequency and yields $k_{CT}^{TA} = 1/1.3\ ps^{-1}$. Our derived charge transfer rate is faster than the few picosecond time constant previously reported in QDs/metal oxide and QDs/Rhenium-polypyridine systems.[37,40]

The encapsulation of QDs in **HP2** not only facilitates charge transfer that has strong implications for their potential usage in photocatalysis but also modifies the QDs' relaxation and recombination dynamics that are intimately related to their use in energy conversion technologies.[41] In 2DES measurements, we extract the homogeneous and inhomogeneous linewidths of the QDs resonance for both samples (Figure 7d).[42] The QDs and **HP2**⊃QDs have similar inhomogeneous linewidths of 35 meV ($1/19\ fs^{-1}$) and 37 meV ($1/18\ fs^{-1}$), respectively, which indicates that **HP2** does not meaningfully increase the local environmental inhomogeneities felt by the QDs. Conversely, the homogeneous linewidth increases from 36 meV ($1/18\ fs^{-1}$) to 45 meV ($1/15\ fs^{-1}$) upon encapsulation. This suggests that the dephasing rate of the excitons increases by 25%, which is predominantly caused by an increase in exciton-phonon scattering rates.[43] We posit that this more efficient exciton-phonon coupling is mediated by the high-density vibrational modes supplied by the **HP2** cavities. These vibrational modes, overlapping in energy with many of the lattice phonon modes in the QDs (see Figure S69 for infrared absorption and Raman spectra), constitute a chaotic, dephasing bath that helps promote the dissipation of the excess electronic energy in the QDs.[44] This effect, in combination with the charge transfer process, accounts for the universal increase in the decay and dephasing rates of the encapsulated QDs across femtosecond to nanosecond timescales.

CONCLUSIONS

In this work, we constructed water-soluble metallo-supramolecular prisms by introducing long, hydrophilic PEG chains onto the backbone of the pentatopic TPY-based ligands. Upon

https://doi.org/10.1021/jacs.2c11981
J. Am. Chem. Soc. 2023, 145, 5191−5202

self-assembly, the resultant prismatic cavity solvates, confines, and completely encapsulates hydrophobic QDs of suitable diameters. Using a suite of optical techniques, we showed that the host profoundly influences the dynamics of its QD guest. The host both injects photoexcited charges into the QDs and universally increases the QDs' ability to dissipate energy to its environment. These endeavors increase the observed size limit of guests from fullerenes (∼1 nm diameter) to inorganic nanocrystals (2−5 nm diameter). This work further demonstrates the ability of a host cavity to alter the optical properties of its non-covalently attached inorganic guest.

In one of our ongoing studies, we are focusing on investigating different QDs with various surface ligands to understand the driving force more deeply in the host−guest system, as well as the different photophysical features of the corresponding **HP2**⊃QD complexes. Further efforts will also focus on tuning the geometry of the hydrophobic interior to investigate how cavity shape and size influence the guests' optical properties.

■ ASSOCIATED CONTENT

Supporting Information

The Supporting Information is available free of charge at https://pubs.acs.org/doi/10.1021/jacs.2c11981.

Experimental procedures and characterization of the new compounds (PDF)

■ AUTHOR INFORMATION

Corresponding Authors

Heng Wang − *College of Chemistry and Environmental Engineering, Shenzhen University, Shenzhen, Guangdong 518060, China;* orcid.org/0000-0002-6829-7205; Email: hengwang@szu.edu.cn

Xuedan Ma − *Center for Nanoscale Materials, Argonne National Laboratory, Lemont, Illinois 60439, United States; Center for Molecular Quantum Transduction, Northwestern-Argonne Institute of Science and Engineering, Evanston, Illinois 60208, United States; Consortium for Advanced Science and Engineering, University of Chicago, Chicago, Illinois 60637, United States;* orcid.org/0000-0002-3163-1249; Email: xuedan.ma@anl.gov

Xiaopeng Li − *College of Chemistry and Environmental Engineering, Shenzhen University, Shenzhen, Guangdong 518060, China; Shenzhen University General Hospital, Shenzhen University Clinical Medical Academy, Shenzhen University, Shenzhen, Guangdong 518055, China;* orcid.org/0000-0001-9655-9551; Email: xiaopengli@szu.edu.cn

Authors

Shuai Lu − *College of Chemistry and Environmental Engineering, Shenzhen University, Shenzhen, Guangdong 518060, China; Institute of Microscale Optoelectronics, Shenzhen University, Shenzhen, Guangdong 518060, China*

Darien J. Morrow − *Center for Nanoscale Materials, Argonne National Laboratory, Lemont, Illinois 60439, United States;* orcid.org/0000-0002-8922-8049

Zhikai Li − *College of Chemistry and Environmental Engineering, Shenzhen University, Shenzhen, Guangdong 518060, China;* orcid.org/0000-0002-9781-2747

Chenxing Guo − *College of Chemistry and Environmental Engineering, Shenzhen University, Shenzhen, Guangdong 518060, China;* orcid.org/0000-0001-6640-6941

Xiujun Yu − *College of Chemistry and Environmental Engineering, Shenzhen University, Shenzhen, Guangdong 518060, China;* orcid.org/0000-0003-4976-8312

Jonathan D. Schultz − *Department of Chemistry and Institute for Sustainability and Energy at Northwestern, Northwestern University, Evanston, Illinois 60208, United States;* orcid.org/0000-0002-3386-5460

James P. O'Connor − *Department of Chemistry and Institute for Sustainability and Energy at Northwestern, Northwestern University, Evanston, Illinois 60208, United States;* orcid.org/0000-0002-8586-9842

Na Jin − *Department of Chemistry, Brown University, Providence, Rhode Island 02912, United States*

Fang Fang − *Instrumental Analysis Center, Shenzhen University, Shenzhen, Guangdong 518060, China*

Wu Wang − *Department of Physics, Southern University of Science and Technology, Shenzhen, Guangdong 518055, China*

Ran Cui − *Key Laboratory of Analytical Chemistry for Biology and Medicine, College of Chemistry and Molecular Sciences, Wuhan University, Wuhan, Hubei 430072, China;* orcid.org/0000-0002-1758-4802

Ou Chen − *Department of Chemistry, Brown University, Providence, Rhode Island 02912, United States;* orcid.org/0000-0003-0551-090X

Chenliang Su − *Institute of Microscale Optoelectronics, Shenzhen University, Shenzhen, Guangdong 518060, China;* orcid.org/0000-0002-8453-1938

Michael R. Wasielewski − *Department of Chemistry and Institute for Sustainability and Energy at Northwestern, Northwestern University, Evanston, Illinois 60208, United States;* orcid.org/0000-0003-2920-5440

Complete contact information is available at: https://pubs.acs.org/10.1021/jacs.2c11981

Author Contributions

‡‡S.L. and D.J.M. contributed equally to the work.

Notes

The authors declare no competing financial interest.

■ ACKNOWLEDGMENTS

This work was financially supported by the National Natural Science Foundation of China (22125106 to X.L. and 22001176 to H.W.), and the Developmental Fund for Science and Technology of Shenzhen (RCJC20200714114556036 to X.L.; 20200812104046002 and RCYX20210706092044070 to H.W.). J.D.S., J.P.O., X.M., and M.R.W. acknowledge support from the Center for Molecular Quantum Transduction, an Energy Frontier Research Center funded by the U.S. Department of Energy, Office of Science, Office of Basic Energy Sciences, under award no. DE-SC0021314 (optical measurements). Work performed at the Center for Nanoscale Materials, a U.S. Department of Energy Office of Science User Facility, was supported by the U.S. DOE, Office of Basic Energy Sciences, under Contract no. DE-AC02-06CH11357. We also thank the Instrument Analysis Center of Shenzhen University for the usage of the TEM instrument.

REFERENCES

(1) (a) Pedersen, C. J. Cyclic polyethers and their complexes with metal salts. *J. Am. Chem. Soc.* **1967**, *89*, 7017−7036. (b) Pedersen, C. J. The discovery of crown ethers (Noble lecture). *Angew. Chem., Int. Ed. Engl.* **1988**, *27*, 1021−1027.

(2) Crini, G. Review: a history of cyclodextrins. *Chem. Rev.* **2014**, *114*, 10940−10975.

(3) Gutsche, C. D. Calixarenes. *Acc. Chem. Res.* **1983**, *16*, 161−170.

(4) (a) Lagona, J.; Mukhopadhyay, P.; Chakrabarti, S.; Isaacs, L. The cucurbit[*n*]uril family. *Angew. Chem., Int. Ed.* **2005**, *44*, 4844−4870. (b) Kim, K.; Selvapalam, N.; Ko, Y. H.; Park, K. M.; Kim, D.; Kim, J. Functionalized cucurbiturils and their applications. *Chem. Soc. Rev.* **2007**, *36*, 267−279.

(5) Ogoshi, T.; Kanai, S.; Fujinami, S.; Yamagishi, T.-a.; Nakamoto, Y. *para*-Bridged symmetrical pillar[5]arenes: their lewis acid catalyzed synthesis and host−guest property. *J. Am. Chem. Soc.* **2008**, *130*, 5022−5023.

(6) (a) Dietrich, B.; Lehn, J. M.; Sauvage, J. P. Les cryptates. *Tetrahedron Lett.* **1969**, *10*, 2889−2892. (b) Lehn, J.-M. Supramolecular chemistry—scope and perspectives molecules, supermolecules, and molecular devices (Noble lecture). *Angew. Chem., Int. Ed. Engl.* **1988**, *27*, 89−112.

(7) (a) Cram, D. J.; Kaneda, T.; Lein, G. M.; Helgeson, R. C. A spherand containing an enforced cavity that selectively binds lithium and sodium ions. *J. Chem. Soc., Chem. Commun.* **1979**, *1979*, 948−950. (b) Cram, D. J. The design of molecular hosts, guests, and their complexes (Noble lecture). *Angew. Chem., Int. Ed. Engl.* **1988**, *27*, 1009−1020.

(8) Ashton, P. R.; Isaacs, N. S.; Kohnke, F. H.; D'Alcontres, G. S.; Stoddart, J. F. Trinacrene-a product of structure-directed synthesis. *Angew. Chem., Int. Ed. Engl.* **1989**, *28*, 1261−1263.

(9) Hasell, T.; Cooper, A. I. Porous organic cages: soluble, modular and molecular pores. *Nat. Rev. Mater.* **2016**, *1*, 16053.

(10) Liu, W.; Stoddart, J. F. Emergent behavior in nanoconfined molecular containers. *Chem* **2021**, *7*, 919−947.

(11) (a) Branda, N.; Wyler, R.; Rebek, J. Encapsulation of methane and other small molecules in a self-assembling superstructure. *Science* **1993**, *263*, 1267−1268. (b) Kusukawa, T.; Fujita, M. Self-assembled M_6L_4-type coordination nanocage with 2,2'-bipyridine ancillary ligands. Facile crystallization and X-ray analysis of shape-selective enclathration of neutral guests in the cage. *J. Am. Chem. Soc.* **2002**, *124*, 13576−13582. (c) Kumazawa, K.; Biradha, K.; Kusukawa, T.; Okano, T.; Fujita, M. Multicomponent assembly of a pyrazine-pillared coordination cage that selectively binds planar guests by intercalation. *Angew. Chem., Int. Ed.* **2003**, *42*, 3909−3913. (d) Yoshizawa, M.; Tamura, M.; Fujita, M. Diels-Alder in aqueous molecular hosts: unusual regioselectivity and efficient catalysis. *Science* **2006**, *312*, 251−254. (e) Mal, P.; Breiner, B.; Rissanen, K.; Nitschke, J. R. White phosphorus is air-stable within a self-assembled tetrahedral capsule. *Science* **2009**, *324*, 1697−1699. (f) Mirtschin, S.; Slabon-Turski, A.; Scopelliti, R.; Velders, A. H.; Severin, K. A coordination cage with an adaptable cavity size. *J. Am. Chem. Soc.* **2010**, *132*, 14004−14005. (g) O'Sullivan, M. C.; Sprafke, J. K.; Kondratuk, D. V.; Rinfray, C.; Claridge, T. D.; Saywell, A.; Blunt, M. O.; O'Shea, J. N.; Beton, P. H.; Malfois, M.; Anderson, H. L. Vernier templating and synthesis of a 12-porphyrin nano-ring. *Nature* **2011**, *469*, 72−75. (h) Yu, G.; Xue, M.; Zhang, Z.; Li, J.; Han, C.; Huang, F. A water-soluble pillar[6]arene: synthesis, host−guest chemistry, and its application in dispersion of multiwalled carbon nanotubes in water. *J. Am. Chem. Soc.* **2012**, *134*, 13248−13251. (i) Dale, E. J.; Vermeulen, N. A.; Thomas, A. A.; Barnes, J. C.; Juríček, M.; Blackburn, A. K.; Strutt, N. L.; Sarjeant, A. A.; Stern, C. L.; Denmark, S. E.; Stoddart, J. F. ExCage. *J. Am. Chem. Soc.* **2014**, *136*, 10669−10682. (j) Kaphan, D. M.; Levin, M. D.; Bergman, R. G.; Raymond, K. N.; Toste, F. D. A supramolecular microenvironment strategy for transition metal catalysis. *Science* **2015**, *350*, 1235−1238. (k) Yazaki, K.; Akita, M.; Prusty, S.; Chand, D. K.; Kikuchi, T.; Sato, H.; Yoshizawa, M. Polyaromatic molecular peanuts. *Nat. Commun.* **2017**, *8*, 15914. (l) Gao, W.-X.; Fan, Q.-J.; Lin, Y.-J.; Jin, G.-X. Control of heterometallic three-dimensional macrocycles with aromatic stacks in tunable host cavities. *Chin. J. Chem.* **2018**, *36*, 594−598. (m) Samanta, D.; Gemen, J.; Chu, Z.; Diskin-Posner, Y.; Shimon, L. J. W.; Klajn, R. Reversible photoswitching of encapsulated azobenzenes in water. *Proc. Natl. Acad. Sci. U.S.A.* **2018**, *115*, 9379−9384. (n) Cai, L.-X.; Li, S.-C.; Yan, D.-N.; Zhou, L.-P.; Guo, F.; Sun, Q.-F. Water-soluble redox-active cage hosting polyoxometalates for selective desulfurization catalysis. *J. Am. Chem. Soc.* **2018**, *140*, 4869−4876. (o) Koo, J.; Kim, I.; Kim, Y.; Cho, D.; Hwang, I.-C.; Mukhopadhyay, R. D.; Song, H.; Ko, Y. H.; Dhamija, A.; Lee, H.; Hwang, W.; Kim, S.; Baik, M.-H.; Kim, K. Gigantic porphyrinic cages. *Chem* **2020**, *6*, 3374−3384. (p) Huang, Q.-C.; Quan, M.; Yao, H.; Yang, L.-P.; Jiang, W. Selective recognition of quaternary ammonium ions by structurally flexible cages. *Chin. J. Chem.* **2021**, *39*, 1593−1598.

(12) (a) Hasenknopf, B.; Lehn, J.-M.; Boumediene, N.; Dupont-Gervais, A.; Van Dorsselaer, A.; Kneisel, B.; Fenske, D. Self-assembly of tetra- and hexanuclear circular helicates. *J. Am. Chem. Soc.* **1997**, *119*, 10956−10962. (b) Isaacs, L.; Park, S.-K.; Liu, S.; Ko, Y. H.; Selvapalam, N.; Kim, Y.; Kim, H.; Zavalij, P. Y.; Kim, G.-H.; Lee, H.-S.; Kim, K. The inverted cucurbit[n]uril family. *J. Am. Chem. Soc.* **2005**, *127*, 18000−18001. (c) Park, J. S.; Karnas, E.; Ohkubo, K.; Chen, P.; Kadish, K. M.; Fukuzumi, S.; Bielawski, C. W.; Hudnall, T. W.; Lynch, V. M.; Sessler, J. L. Ion-mediated electron transfer in a supramolecular donor-acceptor ensemble. *Science* **2010**, *329*, 1324−1327. (d) Riddell, I. A.; Smulders, M. M. J.; Clegg, J. K.; Hristova, Y. R.; Breiner, B.; Thoburn, J. D.; Nitschke, J. R. Anion-induced reconstitution of a self-assembling system to express a chloride-binding $Co_{10}L_{15}$ pentagonal prism. *Nat. Chem.* **2012**, *4*, 751−756. (e) Clever, G. H.; Kawamura, W.; Tashiro, S.; Shiro, M.; Shionoya, M. Stacked platinum complexes of the magnus' salt type inside a coordination cage. *Angew. Chem., Int. Ed.* **2012**, *51*, 2606−2609. (f) Lee, S.; Chen, C.-H.; Flood, A. H. A pentagonal cyanostar macrocycle with cyanostilbene CH donors binds anions and forms dialkylphosphate[3]rotaxanes. *Nat. Chem.* **2013**, *5*, 704−710. (g) Löffler, S.; Lübben, J.; Krause, L.; Stalke, D.; Dittrich, B.; Clever, G. H. Triggered exchange of anionic for neutral guests inside a cationic coordination cage. *J. Am. Chem. Soc.* **2015**, *137*, 1060−1063. (h) Marcos, V.; Stephens, A. J.; Jaramillo-Garcia, J.; Nussbaumer, A. L.; Woltering, S. L.; Valero, A.; Lemonnier, J.-F.; Vitorica-Yrezabal, I. J.; Leigh, D. A. Allosteric initiation and regulation of catalysis with a molecular knot. *Science* **2016**, *352*, 1555−1559. (i) Zhang, T.; Zhou, L.-P.; Guo, X.-Q.; Cai, L.-X.; Sun, Q.-F. Adaptive self-assembly and induced-fit transformations of anion-binding metal-organic macrocycles. *Nat. Commun.* **2017**, *8*, 15898. (j) Cai, K.; Lipke, M. C.; Liu, Z.; Nelson, J.; Cheng, T.; Shi, Y.; Cheng, C.; Shen, D.; Han, J.-M.; Vemuri, S.; Feng, Y.; Stern, C. L.; Goddard, W. A., III; Wasielewski, M. R.; Stoddart, J. F. Molecular Russian dolls. *Nat. Commun.* **2018**, *9*, 5275. (k) Liu, Y.; Zhao, W.; Chen, C.-H.; Flood, A. H. Chloride capture using a C−H hydrogen-bonding cage. *Science* **2019**, *365*, 159−161. (l) Chi, X.; Cen, W.; Queenan, J. A.; Long, L.; Lynch, V. M.; Khashab, N. M.; Sessler, J. L. Azobenzene-bridged expanded "Texas-sized" box: a dual-responsive receptor for aryl dianion encapsulation. *J. Am. Chem. Soc.* **2019**, *141*, 6468−6472.

(13) (a) Kang, J.; Rebek, J. Entropically driven binding in a self-assembling molecular capsule. *Nature* **1996**, *382*, 239−241. (b) MacGillivray, L. R.; Atwood, J. L. A chiral spherical molecular assembly held together by 60 hydrogen bonds. *Nature* **1997**, *389*, 469−472. (c) Beaudoin, D.; Rominger, F.; Mastalerz, M. Chirality-assisted synthesis of a very large octameric hydrogen-bonded capsule. *Angew. Chem., Int. Ed.* **2016**, *55*, 15599−15603.

(14) (a) Olenyuk, B.; Whiteford, J. A.; Fechtenkötter, A.; Stang, P. J. Self-assembly of nanoscale cuboctahedra by coordination chemistry. *Nature* **1999**, *398*, 796−799. (b) Tominaga, M.; Suzuki, K.; Kawano, M.; Kusukawa, T.; Ozeki, T.; Sakamoto, S.; Yamaguchi, K.; Fujita, M. Finite, spherical coordination networks that self-organize from 36 small components. *Angew. Chem., Int. Ed.* **2004**, *43*, 5621−5625. (c) Hiraoka, S.; Harano, K.; Shiro, M.; Ozawa, Y.; Yasuda, N.; Toriumi, K.; Shionoya, M. Isostructural coordination capsules for a series of 10 different d^5-d^{10} transition-metal ions. *Angew. Chem., Int.*

https://doi.org/10.1021/jacs.2c11981
J. Am. Chem. Soc. 2023, 145, 5191−5202

Ed. **2006**, *45*, 6488−6491. (d) Sun, Q.-F.; Iwasa, J.; Ogawa, D.; Ishido, Y.; Sato, S.; Ozeki, T.; Sei, Y.; Yamaguchi, K.; Fujita, M. Self-assembled $M_{24}L_{48}$ polyhedra and their sharp structural switch upon subtle ligand variation. *Science* **2010**, *328*, 1144−1147. (e) Li, K.; Zhang, L.-Y.; Yan, C.; Wei, S.-C.; Pan, M.; Zhang, L.; Su, C.-Y. Stepwise assembly of $Pd_6(RuL_3)_8$ nanoscale rhombododecahedral metal-organic cages via metalloligand strategy for guest trapping and protection. *J. Am. Chem. Soc.* **2014**, *136*, 4456−4459. (f) Xie, T.-Z.; Guo, K.; Guo, Z.; Gao, W.-Y.; Wojtas, L.; Ning, G.-H.; Huang, M.; Lu, X.; Li, J.-Y.; Liao, S.-Y.; Chen, Y.-S.; Moorefield, C. N.; Saunders, M. J.; Cheng, S. Z. D.; Wesdemiotis, C.; Newkome, G. R. Precise molecular fission and fusion: quantitative self-assembly and chemistry of a metallo-cuboctahedron. *Angew. Chem., Int. Ed.* **2015**, *54*, 9224−9229. (g) Yan, X.; Cook, T. R.; Wang, P.; Huang, F.; Stang, P. J. Highly emissive platinum(II) metallacages. *Nat. Chem.* **2015**, *7*, 342−348. (h) Fujita, D.; Ueda, Y.; Sato, S.; Yokoyama, H.; Mizuno, N.; Kumasaka, T.; Fujita, M. Self-assembly of $M_{30}L_{60}$ icosidodecahedron. *Chem* **2016**, *1*, 91−101. (i) Fujita, D.; Ueda, Y.; Sato, S.; Mizuno, N.; Kumasaka, T.; Fujita, M. Self-assembly of tetravalent Goldberg polyhedra from 144 small components. *Nature* **2016**, *540*, 563−566. (j) Rizzuto, F. J.; Nitschke, J. R. Stereochemical plasticity modulates cooperative binding in a $Co^{II}_{12}L_6$ cuboctahedron. *Nat. Chem.* **2017**, *9*, 903−908. (k) Yamashina, M.; Tanaka, Y.; Lavendomme, R.; Ronson, T. K.; Pittelkow, M.; Nitschke, J. R. An antiaromatic-walled nanospace. *Nature* **2019**, *574*, 511−515. (l) Howlader, P.; Zangrando, E.; Mukherjee, P. S. Self-assembly of enantiopure Pd_{12} tetrahedral homochiral nanocages with tetrazole linkers and chiral recognition. *J. Am. Chem. Soc.* **2020**, *142*, 9070−9078. (m) He, L.; Wang, S.-C.; Lin, L.-T.; Cai, J.-Y.; Li, L.; Tu, T.-H.; Chan, Y.-T. Multicomponent metallo-supramolecular nanocapsules assembled from calix[4]resorcinarene-based terpyridine ligands. *J. Am. Chem. Soc.* **2020**, *142*, 7134−7144. (n) Hou, Y.; Zhang, Z.; Lu, S.; Yuan, J.; Zhu, Q.; Chen, W.-P.; Ling, S.; Li, X.; Zheng, Y.-Z.; Zhu, K.; Zhang, M. Highly emissive perylene diimide-based metallacages and their host-guest chemistry for information encryption. *J. Am. Chem. Soc.* **2020**, *142*, 18763−18768. (o) Wang, H.; Wang, K.; Xu, Y.; Wang, W.; Chen, S.; Hart, M.; Wojtas, L.; Zhou, L.-P.; Gan, L.; Yan, X.; Li, Y.; Lee, J.; Ke, X.-S.; Wang, X.-Q.; Zhang, C.-W.; Zhou, S.; Zhai, T.; Yang, H.-B.; Wang, M.; He, J.; Sun, Q.-F.; Xu, B.; Jiao, Y.; Stang, P. J.; Sessler, J. L.; Li, X. Hierarchical self-assembly of nanowires on the surface by metallo-supramolecular truncated cuboctahedra. *J. Am. Chem. Soc.* **2021**, *143*, 5826−5835. (p) Liu, D.; Li, K.; Chen, M.; Zhang, T.; Li, Z.; Yin, J.-F.; He, L.; Wang, J.; Yin, P.; Chan, Y.-T.; Wang, P. Russian-Doll-Like molecular cubes. *J. Am. Chem. Soc.* **2021**, *143*, 2537−2544. (q) Wang, H.; Zhou, L.-P.; Zheng, Y.; Wang, K.; Song, B.; Yan, X.; Wojtas, L.; Wang, X.-Q.; Jiang, X.; Wang, M.; Sun, Q.-F.; Xu, B.; Yang, H.-B.; Sue, A. C.-H.; Chan, Y.-T.; Sessler, J. L.; Jiao, Y.; Stang, P. J.; Li, X. Double-layered supramolecular prisms self-assembled by geometrically non-equivalent tetratopic subunits. *Angew. Chem., Int. Ed.* **2021**, *60*, 1298−1305. (r) He, L.; Hsu, H.-K.; Li, L.; Lin, L.-T.; Tu, T.-H.; Ong, T.-G.; Liou, G.-G.; Chan, Y.-T. A 10-nm-sized multicompartment cuboctahedron and its 2D hierarchical arrays observed by cryo-EM. *Chem* **2022**, *8*, 494−507.

(15) García-Simón, C.; Costas, M.; Ribas, X. Metallosupramolecular receptors for fullerene binding and release. *Chem. Soc. Rev.* **2016**, *45*, 40−62.

(16) (a) Atwood, J. L.; Koutsantonis, G. A.; Raston, C. L. Purification of C_{60} and C_{70} by selective complexation with calixarenes. *Nature* **1994**, *368*, 229−231. (b) Boyd, P. D. W.; Hodgson, M. C.; Rickard, C. E. F.; Oliver, A. G.; Chaker, L.; Brothers, P. J.; Bolskar, R. D.; Tham, F. S.; Reed, C. A. Selective supramolecular porphyrin/fullerene interactions. *J. Am. Chem. Soc.* **1999**, *121*, 10487−10495. (c) Sato, H.; Tashiro, K.; Shinmori, H.; Osuka, A.; Murata, Y.; Komatsu, K.; Aida, T. Positive heterotropic cooperativity for selective guest binding via electronic communications through a fused zinc porphyrin array. *J. Am. Chem. Soc.* **2005**, *127*, 13086−13087. (d) Hajjaj, F.; Tashiro, K.; Nikawa, H.; Mizorogi, N.; Akasaka, T.; Nagase, S.; Furukawa, K.; Kato, T.; Aida, T. Ferromagnetic spin coupling between endohedral metallofullerene La@C_{82} and a cyclodimeric copper porphyrin upon inclusion. *J. Am. Chem. Soc.* **2011**, *133*, 9290−9292. (e) Zhang, C.; Wang, Q.; Long, H.; Zhang, W. A highly C_{70} selective shape-persistent rectangular prism constructed through one-step alkyne metathesis. *J. Am. Chem. Soc.* **2011**, *133*, 20995−21001. (f) Shi, Y.; Cai, K.; Xiao, H.; Liu, Z.; Zhou, J.; Shen, D.; Qiu, Y.; Guo, Q.-H.; Stern, C.; Wasielewski, M. R.; Diederich, F.; Goddard, W. A., III; Stoddart, J. F. Selective extraction of C_{70} by a tetragonal prismatic porphyrin cage. *J. Am. Chem. Soc.* **2018**, *140*, 13835−13842. (g) Yu, X.; Wang, B.; Kim, Y.; Park, J.; Ghosh, S.; Dhara, B.; Mukhopadhyay, R. D.; Koo, J.; Kim, I.; Kim, S.; Hwang, I.-C.; Seki, S.; Guldi, D. M.; Baik, M.-H.; Kim, K. Supramolecular fullerene tetramers concocted with porphyrin boxes enable efficient charge separation and delocalization. *J. Am. Chem. Soc.* **2020**, *142*, 12596−12601.

(17) (a) Ikeda, A.; Yoshimura, M.; Udzu, H.; Fukuhara, C.; Shinkai, S. Inclusion of [60]Fullerene in a homooxacalix[3]arene-based dimeric capsule cross-linked by a Pd^{II}-pyridine interaction. *J. Am. Chem. Soc.* **1999**, *121*, 4296−4297. (b) Suzuki, K.; Takao, K.; Sato, S.; Fujita, M. Coronene nanophase within coordination spheres: increased solubility of C_{60}. *J. Am. Chem. Soc.* **2010**, *132*, 2544−2545. (c) Meng, W.; Breiner, B.; Rissanen, K.; Thoburn, J. D.; Clegg, J. K.; Nitschke, J. R. A self-assembled M_8L_6 cubic cage that selectively encapsulates large aromatic guests. *Angew. Chem., Int. Ed.* **2011**, *50*, 3479−3483. (d) Kishi, N.; Li, Z.; Yoza, K.; Akita, M.; Yoshizawa, M. An M_2L_4 molecular capsule with an anthracene shell: encapsulation of large guests up to 1 nm. *J. Am. Chem. Soc.* **2011**, *133*, 11438−11441. (e) Mahata, K.; Frischmann, P. D.; Würthner, F. Giant electroactive M_4L_6 tetrahedral host self-assembled with Fe(II) vertices and perylene bisimide dye edges. *J. Am. Chem. Soc.* **2013**, *135*, 15656−15661. (f) Nakamura, T.; Ube, H.; Miyake, R.; Shionoya, M. A C_{60}-templated tetrameric porphyrin barrel complex via zinc-mediated self-assembly utilizing labile capping ligands. *J. Am. Chem. Soc.* **2013**, *135*, 18790−18793. (g) García-Simón, C.; Garcia-Borràs, M.; Gómez, L.; Parella, T.; Osuna, S.; Juanhuix, J.; Imaz, I.; Maspoch, D.; Costas, M.; Ribas, X. Sponge-like molecular cage for purification of fullerenes. *Nat. Commun.* **2014**, *5*, 5557. (h) Fuertes-Espinosa, C.; Gómez-Torres, A.; Morales-Martínez, R.; Rodríguez-Fortea, A.; García-Simón, C.; Gándara, F.; Imaz, I.; Juanhuix, J.; Maspoch, D.; Poblet, J. M.; Echegoyen, L.; Ribas, X. Purification of uranium-based endohedral metallofullerenes(EMFs) by selective supramolecular encapsulation and release. *Angew. Chem., Int. Ed.* **2018**, *57*, 11294−11299. (i) Vicent, C.; Martinez-Agramunt, V.; Gandhi, V.; Larriba-Andaluz, C.; Gusev, D. G.; Peris, E. Ion mobility mass spectrometry uncovers guest-induced distortions in a supramolecular organometallic metallosquare. *Angew. Chem., Int. Ed.* **2021**, *60*, 15412−15417.

(18) (a) Fujita, D.; Suzuki, K.; Sato, S.; Yagi-Utsumi, M.; Yamaguchi, Y.; Mizuno, N.; Kumasaka, T.; Takata, M.; Noda, M.; Uchiyama, S.; Kato, K.; Fujita, M. Protein encapsulation within synthetic molecular hosts. *Nat. Commun.* **2012**, *3*, 1093. (b) Fujita, D.; Suzuki, R.; Fujii, Y.; Yamada, M.; Nakama, T.; Matsugami, A.; Hayashi, F.; Weng, J.-K.; Yagi-Utsumi, M.; Fujita, M. Protein stabilization and refolding in a gigantic self-assembled cage. *Chem* **2021**, *7*, 2672−2683.

(19) (a) Suzuki, K.; Sato, S.; Fujita, M. Template synthesis of precisely monodisperse silica nanoparticles within self-assembled organometallic spheres. *Nat. Chem.* **2010**, *2*, 25−29. (b) Ichijo, T.; Sato, S.; Fujita, M. Size-, mass-, and density-controlled preparation of TiO_2 nanoparticles in a spherical coordination template. *J. Am. Chem. Soc.* **2013**, *135*, 6786−6789. (c) Mondal, B.; Mukherjee, P. S. Cage encapsulated gold nanoparticles as heterogeneous photocatalyst for facile and selective reduction of nitroarenes to azo compounds. *J. Am. Chem. Soc.* **2018**, *140*, 12592−12601. (d) Liu, T.; Bai, S.; Zhang, L.; Hahn, F. E.; Han, Y.-F. N-heterocyclic carbene-stabilized metal nanoparticles within porous organic cages for catalytic application. *Natl. Sci. Rev.* **2022**, *9*, nwac067.

(20) Harris, R. D.; Bettis Homan, S.; Kodaimati, M.; He, C.; Nepomnyashchii, A. B.; Swenson, N. K.; Lian, S.; Calzada, R.; Weiss,

https://doi.org/10.1021/jacs.2c11981
J. Am. Chem. Soc. 2023, 145, 5191−5202

E. A. Electronic processes within quantum dot-molecule complexes. *Chem. Rev.* **2016**, *116*, 12865−12919.
(21) Goesmann, H.; Feldmann, C. Nanoparticulate functional materials. *Angew. Chem., Int. Ed.* **2010**, *49*, 1362−1395.
(22) He, H.; Cui, Y.; Li, B.; Wang, B.; Jin, C.; Yu, J.; Yao, L.; Yang, Y.; Chen, B.; Qian, G. Confinement of perovskite-QDs within a single MOF crystal for significantly enhanced multiphoton excited luminescence. *Adv. Mater.* **2019**, *31*, No. e1806897.
(23) Algar, W. R.; Kim, H.; Medintz, I. L.; Hildebrandt, N. Emerging non-traditional Förster resonance energy transfer configurations with semiconductor quantum dots: investigations and applications. *Coord. Chem. Rev.* **2014**, *263*−*264*, 65−85.
(24) (a) Wasielewski, M. R. Self-assembly strategies for integrating light harvesting and charge separation in artificial photosynthetic systems. *Acc. Chem. Res.* **2009**, *42*, 1910−1921. (b) Wolfbeis, O. S. An overview of nanoparticles commonly used in fluorescent bioimaging. *Chem. Soc. Rev.* **2015**, *44*, 4743−4768. (c) Romero, E.; Novoderezhkin, V. I.; van Grondelle, R. Quantum design of photosynthesis for bio-inspired solar-energy conversion. *Nature* **2017**, *543*, 355−365.
(25) Wang, H.; Liu, C.-H.; Wang, K.; Wang, M.; Yu, H.; Kandapal, S.; Brzozowski, R.; Xu, B.; Wang, M.; Lu, S.; Hao, X.-Q.; Eswara, P.; Nieh, M.-P.; Cai, J.; Li, X. Assembling pentatopic terpyridine ligands with three types of coordination moieties into a giant supramolecular hexagonal prism: synthesis, self-assembly, characterization, and antimicrobial study. *J. Am. Chem. Soc.* **2019**, *141*, 16108−16116.
(26) Kalenius, E.; Groessl, M.; Rissanen, K. Ion mobility−mass spectrometry of supramolecular complexes and assemblies. *Nat. Rev. Chem.* **2019**, *3*, 4−14.
(27) (a) Li, X.-B.; Tung, C.-H.; Wu, L.-Z. Semiconducting quantum dots for artificial photosynthesis. *Nat. Rev. Chem.* **2018**, *2*, 160−173. (b) Lu, H.; Huang, Z.; Martinez, M. S.; Johnson, J. C.; Luther, J. M.; Beard, M. C. Transforming energy using quantum dots. *Energy Environ. Sci.* **2020**, *13*, 1347−1376.
(28) Chen, O.; Zhao, J.; Chauhan, V. P.; Cui, J.; Wong, C.; Harris, D. K.; Wei, H.; Han, H.-S.; Fukumura, D.; Jain, R. K.; Bawendi, M. G. Compact high-quality CdSe-CdS core-shell nanocrystals with narrow emission linewidths and suppressed blinking. *Nat. Mater.* **2013**, *12*, 445−451.
(29) Pluth, M. D.; Raymond, K. N. Reversible guest exchange mechanisms in supramolecular host-guest assemblies. *Chem. Soc. Rev.* **2007**, *36*, 161−171.
(30) (a) Yang, F.; Liu, X.; Yang, Z. Chiral metal nanoparticle superlattices enabled by porphyrin-based supramolecular structures. *Angew. Chem., Int. Ed.* **2021**, *60*, 14671−14678. (b) Liu, J.; Liu, R.; Li, H.; Zhang, F.; Yao, Q.; Wei, J.; Yang, Z. Diversifying nanoparticle superstructures and functions enabled by translative templating from supramolecular polymerization. *Angew. Chem., Int. Ed.* **2022**, *61*, No. e202201426. (c) Liu, R.; Feng, Z.; Cheng, C.; Li, H.; Liu, J.; Wei, J.; Yang, Z. Active regulation of supramolecular chirality through integration of CdSe/CdS nanorods for strong and tunable circular polarized luminescence. *J. Am. Chem. Soc.* **2022**, *144*, 2333−2342.
(31) (a) Asbury, J. B.; Hao, E.; Wang, Y.; Ghosh, H. N.; Lian, T. Ultrafast electron transfer dynamics from molecular adsorbates to semiconductor nanocrystalline thin films. *J. Phys. Chem. B* **2001**, *105*, 4545−4557. (b) Alemán, E. A.; Shreiner, C. D.; Rajesh, C. S.; Smith, T.; Garrison, S. A.; Modarelli, D. A. Photoinduced electron-transfer within osmium(II) and ruthenium(II) *bis*-terpyridine donor acceptor dyads. *Dalton Trans.* **2009**, 6562−6577. (c) Jiang, T.; Bai, Y.; Zhang, P.; Han, Q.; Mitzi, D. B.; Therien, M. J. Electronic structure and photophysics of a supermolecular iron complex having a long MLCT-state lifetime and panchromatic absorption. *Proc. Natl. Acad. Sci. U.S.A.* **2020**, *117*, 20430−20437.
(32) Klimov, V. I.; McBranch, D. W.; Leatherdale, C. A.; Bawendi, M. G. Electron and hole relaxation pathways in semiconductor quantum dots. *Phys. Rev. B* **1999**, *60*, 13740−13749.
(33) Petkov, B. K.; Gellen, T. A.; Farfan, C. A.; Carbery, W. P.; Hetzler, B. E.; Trauner, D.; Li, X.; Glover, W. J.; Ulness, D. J.; Turner, D. B. Two-dimensional electronic spectroscopy reveals the spectral dynamics of Förster resonance energy transfer. *Chem* **2019**, *5*, 2111−2125.
(34) Kamoya, Y.; Kojima, K.; Tanaka, G.; Tanaka, R.; Mutai, T.; Araki, K. Propylamino-connected fluorescent terpyridine dimer and trimer: syntheses, photophysical properties and formation of duplex-type complexes with Cd(II). *Org. Biomol. Chem.* **2012**, *10*, 8895−8902.
(35) Empedocles, S. A.; Neuhauser, R.; Bawendi, M. G. Three-dimensional orientation measurements of symmetric single chromophores using polarization microscopy. *Nature* **1999**, *399*, 126−130.
(36) Spinicelli, P.; Buil, S.; Quélin, X.; Mahler, B.; Dubertret, B.; Hermier, J.-P. Bright and grey states in CdSe-CdS nanocrystals exhibiting strongly reduced blinking. *Phys. Rev. Lett.* **2009**, *102*, 136801.
(37) Tvrdy, K.; Frantsuzov, P. A.; Kamat, P. V. Photoinduced electron transfer from semiconductor quantum dots to metal oxide nanoparticles. *Proc. Natl. Acad. Sci. U.S.A.* **2011**, *108*, 29−34.
(38) Wu, D.; Xiao, L.; Shi, Y.; Zhang, Q.; Du, W.; Zhang, J.; Li, S.; Zhou, H.; Wu, J.; Tian, Y. Novel Zn(II)/Cd(II) complexes based on ferrocenyl terpyridine: crystal structures, electrochemical and third-order nonlinear optical properties using tunable femtosecond laser. *J. Organomet. Chem.* **2017**, *830*, 67−73.
(39) Kagan, C. R.; Murray, C. B. Charge transport in strongly coupled quantum dot solids. *Nat. Nanotech.* **2015**, *10*, 1013−1026.
(40) Sykora, M.; Petruska, M. A.; Alstrum-Acevedo, J.; Bezel, I.; Meyer, T. J.; Klimov, V. I. Photoinduced charge transfer between CdSe nanocrystal quantum dots and Ru-polypyridine complexes. *J. Am. Chem. Soc.* **2006**, *128*, 9984−9985.
(41) Caram, J. R.; Zheng, H.; Dahlberg, P. D.; Rolczynski, B. S.; Griffin, G. B.; Fidler, A. F.; Dolzhnikov, D. S.; Talapin, D. V.; Engel, G. S. Persistent inter-excitonic quantum coherence in CdSe quantum dots. *J. Phys. Chem. Lett.* **2014**, *5*, 196−204.
(42) Siemens, M. E.; Moody, G.; Li, H.; Bristow, A. D.; Cundiff, S. T. Resonance lineshapes in two-dimensional Fourier transform spectroscopy. *Opt. Exp.* **2010**, *18*, 17699−17708.
(43) Azzaro, M. S.; Le, A. K.; Wang, H.; Roberts, S. T. Ligand-enhanced energy transport in nanocrystal solids viewed with two-dimensional electronic spectroscopy. *J. Phys. Chem. Lett.* **2019**, *10*, 5602−5608.
(44) (a) Guyot-Sionnest, P.; Wehrenberg, B.; Yu, D. Intraband relaxation in CdSe nanocrystals and the strong influence of the surface ligands. *J. Chem. Phys.* **2005**, *123*, 074709. (b) Kilina, S.; Velizhanin, K. A.; Ivanov, S.; Prezhdo, O. V.; Tretiak, S. Surface ligands increase photoexcitation relaxation rates in CdSe quantum dots. *ACS Nano* **2012**, *6*, 6515−6524.

https://doi.org/10.1021/jacs.2c11981
J. Am. Chem. Soc. 2023, 145, 5191−5202